Application of PVDF foils for the measurements of unsteady pressures on wind tunnel models for the prediction of aircraft vibrations

W. Luber and J. Becker (retired)
EADS-MAS (Military Air System)
85077 Manching, Germany
wolfgang.luber@eads.com

Keywords: Buffet, unsteady aerodynamic pressure, Smart sensors and signal processing

Abstract

An experimental investigation of unsteady pressures on military aircraft wind tunnel models has been performed using Polyvinylidenfluorid (PVDF) sensors. The unsteady pressures from the wind tunnel measurements are a prerequisite for the prediction of dynamic loads and vibrations during the development and design of new fighter aircraft structures. In the past the wind tunnel unsteady pressure measurements had been performed using wind tunnel models equipped by Kulite pressure sensors. This technique resulted in very high cost wind tunnel models. In contrast the application of the PVDF foil Smart Sensor & Signal Processing Technology would lead to improvements through the application of an affordable test technique which could be also applied in flight with the benefit of more accurate and locally detailed pressure information.
The present investigation includes the measurement of unsteady pressures with PVDF foils on a wind tunnel model of a trainer aircraft configuration in the high speed transonic wind tunnel of the NLR Amsterdam. The investigated Mach numbers were M0.5, M0.7 and M0.9 and the incidence range was 0 to 45 degrees. The results of the experiments are discussed using the analysed time histories and power spectral densities of the stochastic unsteady pressure and comparisons to results using direct unsteady pressure measurements. Main aspect is the evaluation and validation with respect to technical industrial applicability of PVDF foils.

1. Introduction

During the development of military aircraft structural design dynamic loads have to be established which arise from unsteady aerodynamics caused by separated flow on the aircraft at high incidences, so called buffet forces which are essential components of the design and fatigue loads. These periodic and stochastic buffet forces excite the elastic vibration modes of aircraft structural components, leading for instance the wing-, the fin- and horizontal tail buffeting.

Fin-buffeting is an aero-elastic phenomenon occurring on various high performance fighter aircraft. Flying at high angles of attack vortices originate from the leading edges of wing and fuselage. These unsteady vortices which contain fluctuating flow components burst drastically near the vertical tail of the aircraft and exciting the structure of the vertical tail in its natural modes. The resulting buffet fatigue loads can become an airframe fatigue and maintenance problem and might either require a structural design including dynamic buffet loads or heavier structures, excessive inspection or active measures to reduce dynamic structural loads.

In the past buffet forces have been predicted using an experimental technique based on the measurement of wind tunnel models instrumented with a certain number of unsteady pressure pick ups. For instance the wing and fin

buffet loads of several military aircraft have been experimentally derived by application of the unsteady pressure measurement technique, ref. 1 - 10. This technique resulted in very high cost wind tunnel models, for both the development and maintenance of the model.

Another promising technique for the measurement of unsteady pressures has been proposed by several authors, described for example in, ref. 11-13 which is based on the application of the PVDF foil Smart Sensor & Signal Processing Technology.

This technology is especially investigated here on a wind tunnel model of a military trainer aircraft configuration of EADS Military Air System Deutschland.

2. Description of the wind tunnel model tests

2.1 Description of the wind tunnel model

The wind tunnel model is a 1:15 scaled configuration of a military combat aircraft. The design of this Aircraft is driven by the strategic target to combine both a Trainer and a light combat aircraft together. The layout of the Aircraft show that it is a two seat airplane with one engine and the capability to fly supersonic speeds. The basic configuration contains beside the two missiles, mounted on the tip position of the wings also some interface points for carrying underwing external stores like fuel tanks and reconnaissance pods. For aerodynamic purpose the model is similar to the full version and therefore the air intake is built in the scale. This Aircraft has two air intakes on the left and right side of the centre fuselage. Flying in high angle of attack is main point of the design criteria of this aircraft. Due to the fact that this aircraft should fly a very long time with more flight hours compared with a pure fighter aircraft the structure should be designed to withstand all the buffet excitation. The better design would be that the buffet excitation will be minimized. The configuration is shown in Fig. 1.

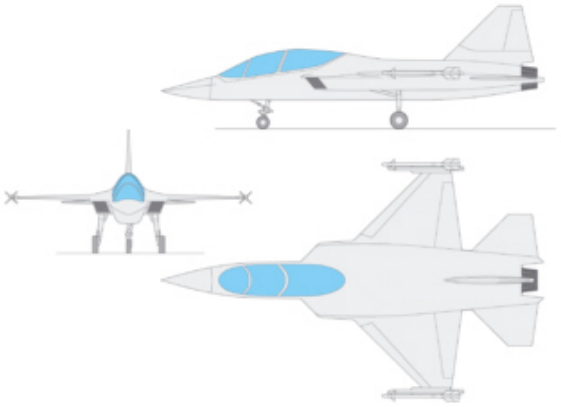

Figure 1: Wind Tunnel Model AT2000

2.2 Description of the wind tunnel model instrumentation

The instrumentation of the fin is shown in figure 2.

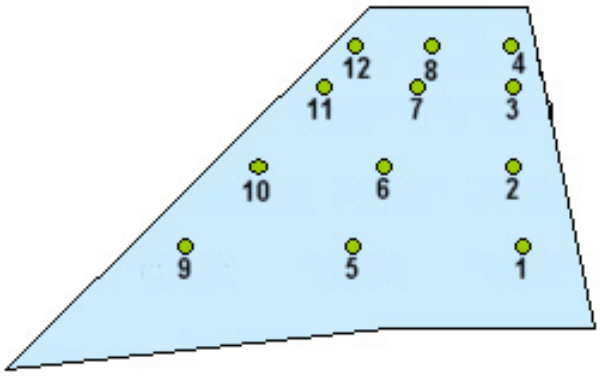

Port Fin, Pick ups distribution 1-12

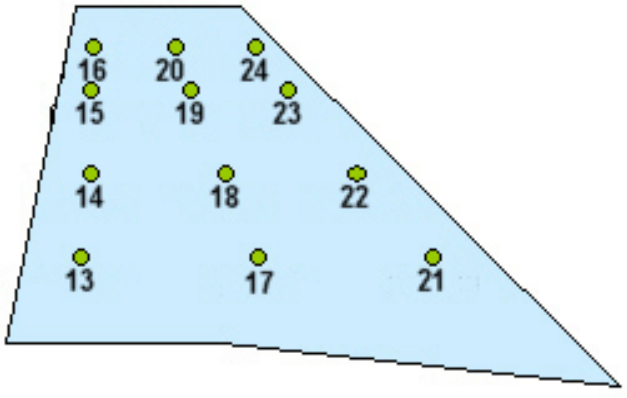

Starboard Fin, Pick ups distribution 13-24

Figure 2: Location of the port and starboard pressure measuring points

The instrumentation was performed by Mirow Systemtechnik GmbH, Berlin. A PVDF foil has been attached at the port and starboard side of the fin. Twelve pressure locations at the port and starboard side have been installed and instrumented at 4 span-wise sections.
The following different configurations of the aircraft can be changed during wind tunnel trials, by using components of the trailing flaps to simulate different deflection angles.

Wing trailing edge flap:

- $\eta_{flap} = -20°;\ -10°;\ 0,\ +10°;\ +20°$

Vertical Tail

- $\eta_{rudder} = 0,\ +10°;\ +20°$

Horizontal Tail:

- $\eta_{HT} = -20°;\ -15°;\ -10°;\ -5°;\ 0,\ +5°;\ +10°;\ +15°;\ +20°$

The on board measurement equipment is installed behind the cockpit in the front fuselage. The cockpit can be removed to maintain the equipment.

Figure 3 shows the complete wind tunnel model installed in the NLR High Speed Tunnel in Amsterdam. The pitch up position of the port vertical tail can be seen very good on the figure. Figure 4 depicts the wiring system of the installed piezos in more detail.

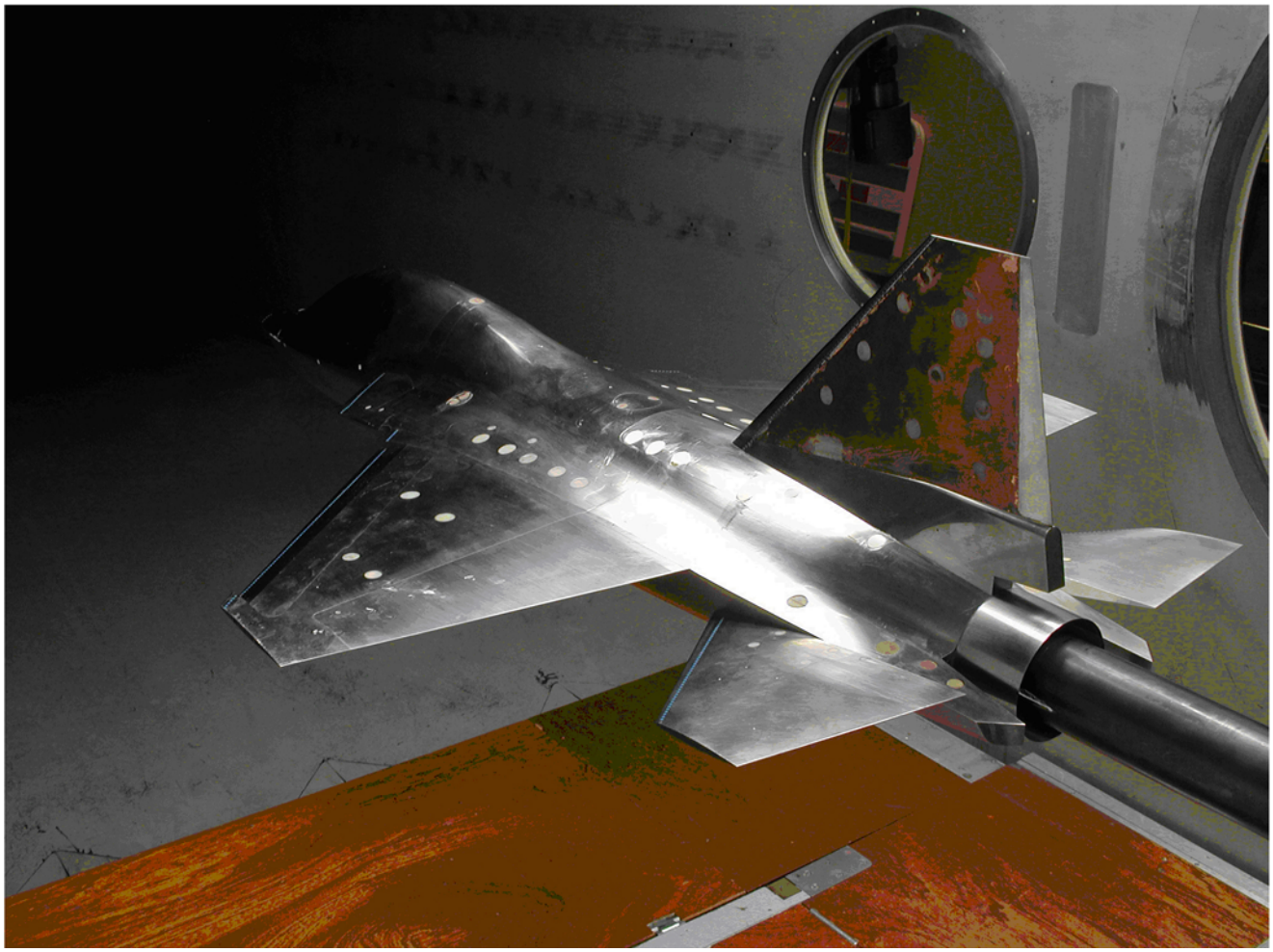

Figure 3: Model in NLR HST wind tunnel – Fin instrumented with PVDF foil

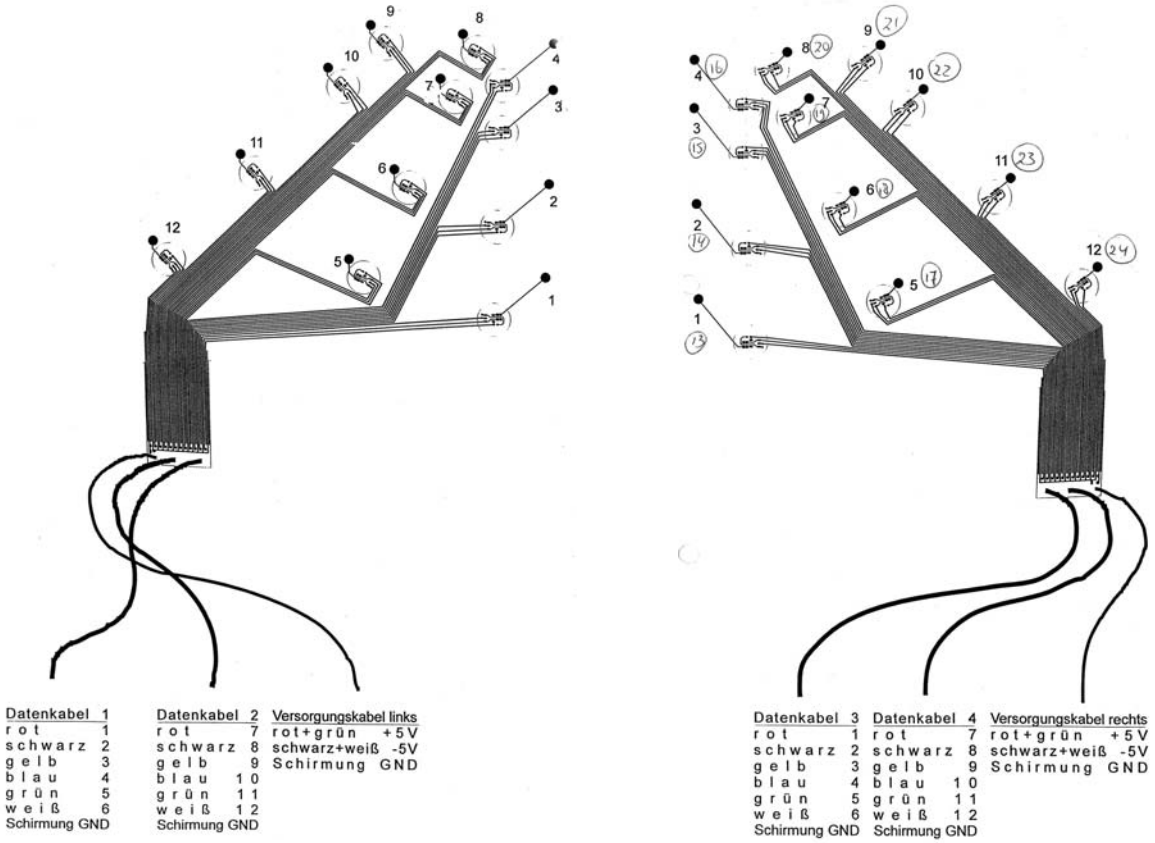

Figure 4: Location of pressure measuring location on port and starboard fin

2.3 Description of the PVDF foil Smart Sensor & Signal Processing Technology

The measuring technique is based on the application of a piezoelectric foil with a discretised sensor structure which is glued onto the airfoil model. The piezo foil is an extremely thin ($9\mu < h < 100\ \mu m$) plastic foil made of PVDF films and is metallized on both sides.

The piezo effect results from the partially crystallized structure of the foil material, which is polarized by high field intensity while solidifying. For this reason the foil reacts with a change of electrical charge proportional to stress which is gripped from the metallized surface and is registered by means of a charge amplifier. The sensors are well suited to be used on airfoils in wind tunnel as well as in free flight test, since their applicability is within a range of temperature between –40 and +150 °C. The high sensitivity of the foils and the small attenuation of the piezo material allow an almost inertia less measurement of unsteady forces. In general several stress factors (shear, pressure and temperature fluctuations) occur in the piezo foil' s measuring signal. The superimposed components can be isolated to a great extent by an appropriate separation technique, see ref. 11. Some PVDF properties are demonstrated in table 1 below.

2.4 Description of the wind tunnel model test program

The test have been performed at the NLR Amsterdam high speed wind tunnel (HST)
Wind tunnel conditions are described in table 2:

Symbol	Parameter	PVDF	Copolymer	Units
t	Thickness	9,28,52,110	<1 to 1200	µm (micron, 10^{-6})
d_{31}	Piezo Strain Constant	23	11	10^{-12} m/m/V/m or C/ m^2/ N/m^2
d_{33}	Piezo Strain Constant	-33	-38	10^{-12} m/m/V/m or C/ m^2/ N/m^2
g_{31}	Piezo Stress Constant	216	162	10^{-3} V/m / N/m^2or m/m/C/ m^2
g_{33}	Piezo Stress Constant	-330	-542	10^{-3} V/m / N/m^2or m/m/C/ m^2
Y	Young's Modulus	2-4	3-5	10^9 N/m^2

Table 1: Typical Properties of piezo film; further details see ref. 11

Flow parameters					
Tunnel speed	U_∞	169	232	290	m/s
Dynamic pressure	q_∞	9900	13200	16000	Pa
Tunnel pressure	p_∞	~950.			Pa
Temperature	T_∞	~20.			Deg. Celsius
Mach number	Ma_∞	0.5	0.7	0.9	-
Reynolds number	$Re_{l\mu}$	0.68×10^6			-
Angle of attack	α	0…15…45 $10 < \alpha < 45; \Delta\alpha = 5$			deg
Side slip angle		0.0			
Sampling rate	f_M	2000			Hz
Low pass frequency	f_T	256			Hz
Test time	t_M	20			s

Table 2: Wind tunnel test conditions

3. Test results

3.1 Evaluation of time histories, rms values and power spectral densities of unsteady fin buffet pressures

3.1.1 Unsteady pressures

Time histories of the surface pressure p(l, t) at the different locations are recorded during the tests. Non-dimensional pressure coefficients are defined as:

$$c_p(1,t) = \frac{p(1,t) - p_\infty}{q_\infty}$$

and the mean pressure values $c_p(l)$ at the location l are:

$$\bar{c}_p(1) = \frac{1}{T}\int c_p(1,t)\cdot dt$$

T is the test duration. The mean square value is defined by

$$\bar{c}_p^2(1) = \frac{1}{T}\int \left[c_p(1,t) - \bar{c}_p(1)\right]^2 dt$$

and the rms (root mean square) value is $\sqrt{\bar{c}_p^2(1)}$

3.1.2 Time histories

Figures 6 - 9 show typical time histories of measuring point MP9 for different angles of attack.

3.1.3 RMS pressures

RMS pressures in [Pa] for the locations MP1, MP2, MP6, MP8, MP9, MP11 and MP12 are analyzed and non dimensional rms pressure coefficients are compared as function of angle of attack in figure 5.

These Figures demonstrate the comparison of the rms pressure coefficients of the locations MP1, MP2, MP8, MP9, MP11, MP12 versus incidence.

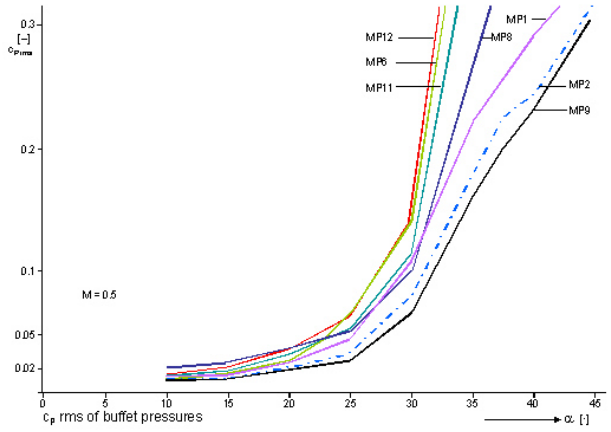

Figure 5: RMS values of pressure coefficients

3.1.4 Power spectral densities

In the next figures power spectral densities, as well as the power spectra are depicted.

3.1.4.1 Peak frequencies in the power spectra densities

The comparison of the spectra of different location show very similar behaviour of peaks. Dominant peaks occur always around 380 and 405 Hz and around 920 Hz. The first two peak frequencies correspond to the well know vortex shedding phenomenon behind the wing of an aircraft configuration at higher incidences, known for example from the Eurofighter configuration, which is characterized by a periodic process as also known as von Karman vortex street behind cylinders. It is interesting to detect two similar frequencies which indicates a fine resolution of the signals by the PVDF foil technique. The peak frequencies are found to be identical for all locations and for all incidences.

Reduced frequencies $k = fl_\mu/U\infty$ of the two first peak frequencies are: k =0.54 and 0.575 (l_μ = 0.24 m). The amplitude of the first peak is always significantly higher. The peak frequency at 920 Hz might result from another vortex shedding phenomenon, the origin of which is not known but might be caused by the front fuselage. Peaks from motion induced unsteady pressures are believed to be of minor importance.

3.1.4.2 Effect of pressure signal location

The peak amplitudes in the spectral densities and the power spectra vary to some extent for the different locations. This was already previously demonstrated by the rms values in figure 5. The effect of location is shown through the figures 6 to 9 for the locations MP8 at 37.5 degrees, for location MP8, MP9 and MP11 at 10 degrees.

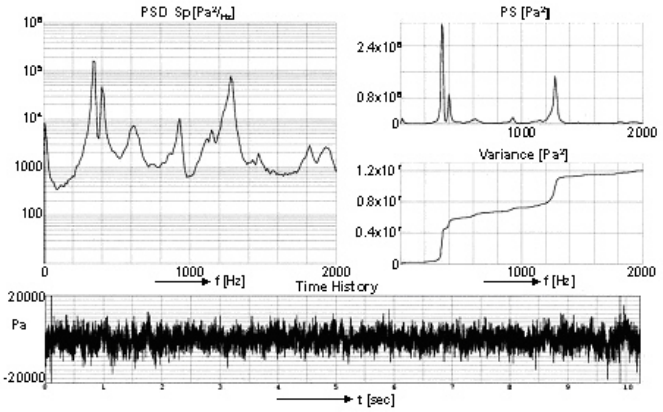

Figure 6: Power spectral density, power spectrum variance and time history of pressure MP8 at 37.5 degrees

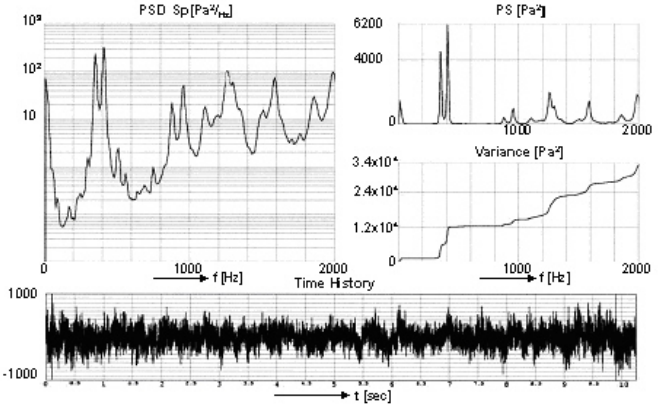

Figure 7 : Power spectral density, power spectrum variance and time history of pressure MP8 at 10 degrees

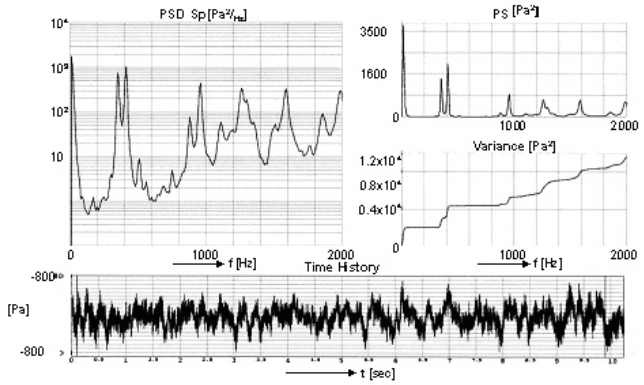

Figure 8: Power spectral density, power spectrum variance and time history of pressure MP9 at 10 degrees

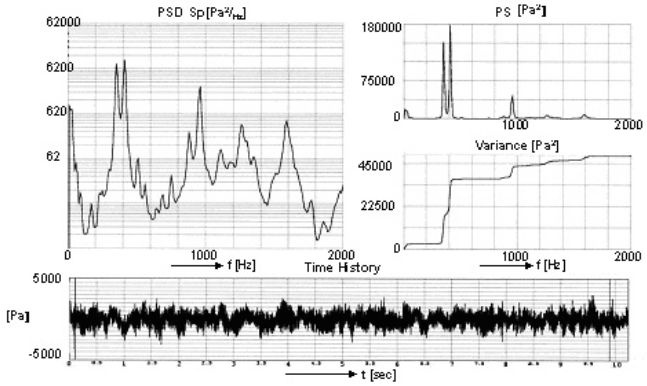

Figure 9: Power spectral density, power spectrum variance and time history of pressure MP11 at 10 degrees

3.1.4.3 Effect of model incidence

The power spectra densities and power spectra and rms values of the buffet pressures increase with incidence. From 0 to 10 degrees the increase is moderate. Beyond 15 degrees an increasingly stronger magnitude development is found, as shown in the figures 10, 11. The increase with incidence is seen especially at the frequency of about 400 Hz corresponding to a reduced frequency of ~ 0.6.

3.2 Conclusion of PVDF foil measurements

All expected trends of fin buffet pressures which are known from other aircraft configurations are found through the measurement with PVDF foils. Especially the trend of the rms values with incidence, the characteristic peaks in the power spectra and the development of the rms values and the power spectra are similar to the results on other configurations. The resolution of the signals with amplitude and frequency is judged to be accurate.

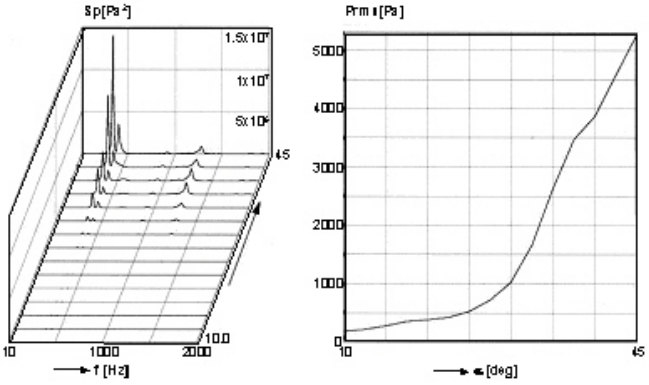

Figure 10: Power Spectra S_p [Pa^2] and rms of pressure signal position MP8 at Mach 0.5 as function of incidence

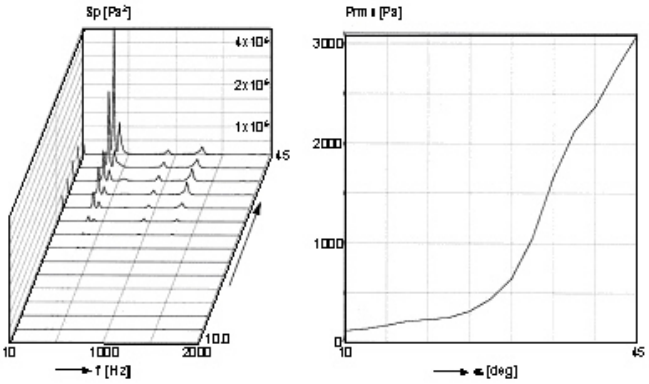

Figure 11: Power Spectra S_p [Pa^2] and rms of pressure signal position MP9 at Mach 0.5 as function of incidence

4. Validation of the PVDF foil Smart Sensor & Signal Processing Technology

It is intended to validate the PVDF foil Smart Sensor & Signal Processing Technology for the measurement of unsteady aerodynamic fin buffet pressures through a comparison with results from classical wind tunnel model measurements of unsteady pressures using Kulite pressure pick ups on the same model.
For the comparison of the PVDF unsteady fin pressures described in chapter 3 wind tunnel measurements with the same model but with pressure pickups (Kulites) installed on the fin have been performed using the low speed wind tunnel of the Technical University of Munich – Institute of Aerodynamics. The measurement was initiated and supported by EADS Military Air Systems. The model, see fig. 12 the instrumentation and the test results are described below.

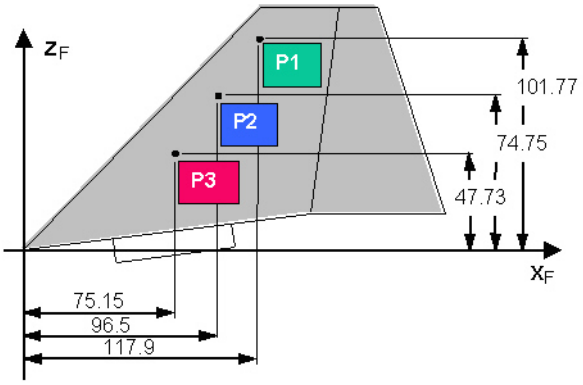

Figure 12: TUM test Location of pressure pick ups

4.1 Description of the wind tunnel tests using pressure pick ups on the fin (TUM test)

In figure 12 the wind tunnel model which was used at Technical University Munch for validation of the measurements are shown with the three unsteady pick up position.

4.1.1 Description of the experimental technique and the test program

The following test parameters characterize the pressure measurements for the 1:15 scaled AT2000- high speed model in figure 12 and described in table 3

Flow parameters			
Tunnel speed	U_∞	40.0	m/s
Dynamic pressure	q_∞	~890.	Pa
Tunnel pressure	p_∞	~950.	Pa
Temperature	T_∞	~20.	Deg. Celsius
Mach number	Ma_∞	0.118	-
Reynolds number	$Re_{l\mu}$	0.68×10^6	-
Angle of attack	α	0…15…30 $0 < \alpha < 10$, $\Delta\alpha = 5$ $10 < \alpha < 20$, $\Delta\alpha = 2$ $20 < \alpha < 30$, $\Delta\alpha = 1$	deg
Side slip angle		0.0	

Signal parameters			
Sampling rate	f_M	2000	Hz
Low pass frequency	f_T	256	Hz
Test time	t_M	15	s
Block samples	N	30000	

Table 3: TUM wind tunnel measurement test parameters

4.1.2 Unsteady pressures

Time histories of the surface pressure p(l, t) at the different locations l are recorded during the tests. Non-dimensional pressure coefficients are defined as:

$$c_p(1,t) = \frac{p(1,t) - p_\infty}{q_\infty}$$

and the mean pressure values $c_p(l)$ at the location l are:

$$\bar{c}_p(1) = \frac{1}{T}\int c_p(1,t)\cdot dt$$

T is the test duration. The mean square value is defined by

$$\bar{c}_p^2(1) = \frac{1}{T}\int \left[c_p(1,t) - \bar{c}_p(1)\right]^2 dt$$

and the rms (root mean square) value is $\sqrt{\bar{c}_p^2(1)}$

The power spectral density of the fluctuating pressure coefficient is defined by the conjugate complex multiplication of the complex values of the Fourier transform F (l,ω) of the fluctuating pressures coefficients at the location l:

$$S_{cp}(1,\omega) = \lim\frac{2}{T}F^*(1,\omega)\cdot F(1,\omega)$$

introducing the reduced frequency $k = \frac{f\cdot\bar{c}}{U_\infty}$

the non-dimensional form of the power spectral density S_{cp}^N

$$S_{cp}^N(1,k) = \frac{U_\infty}{\bar{c}} S_{cp}(1,k)$$

The non-dimensional power spectral density can be transformed into an amplitude spectral density

$$c_p^A(1,k) = \sqrt{2\cdot S_{cp}^N(1,k)\Delta k} \quad \text{where} \quad \Delta k = \frac{\Delta f\cdot\bar{c}}{U_\infty}$$

is.

4.2 Results of the TUM measurement

The classical measurement of buffet pressures using Kulites has already been validated in the past by the Technical University of Munch (TUM) Institute of Aerodynamic, Ref. 4 – 6.
The time histories of the fin buffet pressures from the TUM wind tunnel measurement with the military trainer aircraft configuration have been evaluated for the angle of attack region 0 to 30°. A low pass filter has been applied with a cut off frequency of 256 Hz. Root mean square values of the non dimensional pressure coefficients for the filtered signals at the locations P1, P2 and P3 and amplitude power spectra have been generated .
Fig. 13 shows the development of the c_{prms} values of the signals at P1, P2 and P3. A strong increase of the rms values are present beyond 20°. All three signals show a very similar trend with incidence, this well known trend is also present at the fin of different aircraft configurations.

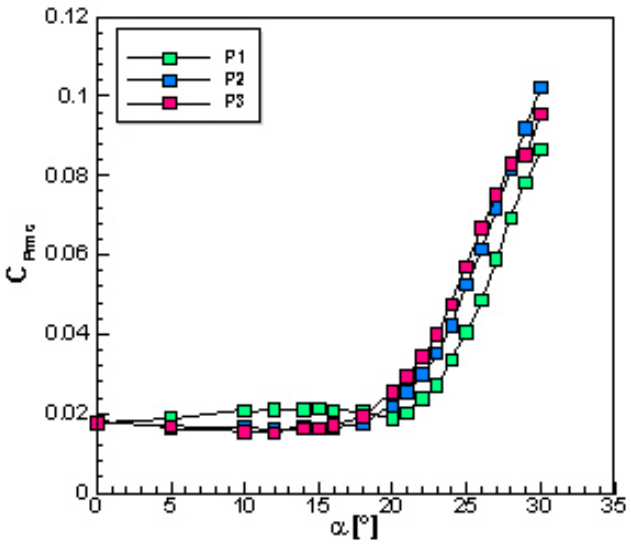

Figure 13: TUM test - Root mean square values of the unsteady fin pressures at the location P1, P2 and P3 as function of angle of attack

The amplitude power spectra of the signal at P1 is depicted in fig. 14 below for the different angle of attacks. A pronounced peak occurs at a reduced frequency of ~ 0.6. This peak increases with incidence and reaches a maximum value at 30 °. The development beyond 30°.

Is not known from these measurements. This reduced frequency corresponds to the vortex shedding frequency of the wing.

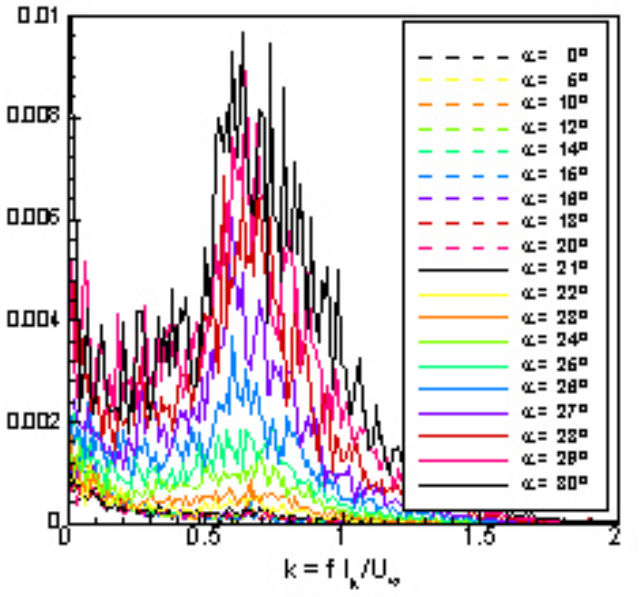

Figure 14: TUM test - Amplitude power spectra of the pressure at P1 as function of angle of attack

4.3 Comparison of the test results from PVDF foil measurements and pressure pick up measurements

4.3.1 Comparison with results of a different aircraft configuration

Results of buffet measurements on the fin of a canard delta configuration are shown below.

The trend of the rms values versus incidence are similar to the results of the NLR trainer tests. The power spectra of a fin signal (P13) show peak values at a reduced frequency of about 0.6 similar to the NLR trainer buffet pressure spectra. This comparison gives confidence in the trends of the PVDF foil test results.

4.3.2 Comparison of PVDF test results with results from TUM experiments for the trainer configuration

Experimental buffet investigations performed in the past on the Eurofighter configuration have demonstrated that low speed buffet measurements at Mach ~ 0.1 can be applied for the prediction of buffet pressures at Mach number up to Mach 0.8, Ref. 4-6.

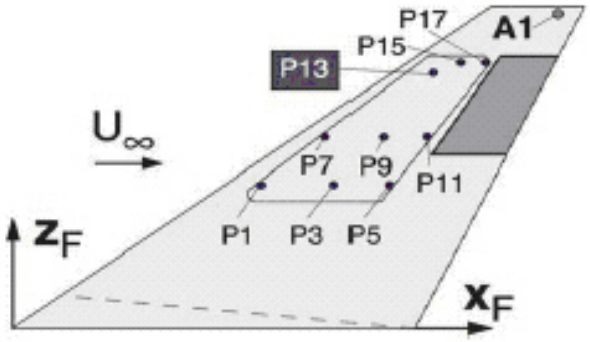

Figure 15: Pick ups for fin pressure measurement

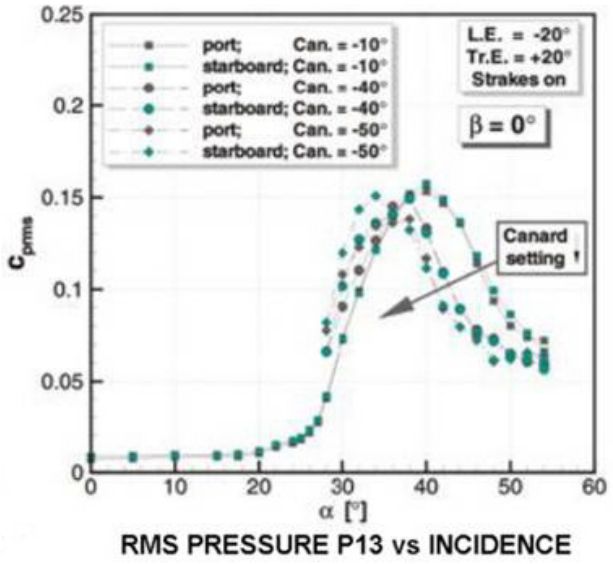

Figure 16: RMS pressure versus incidence

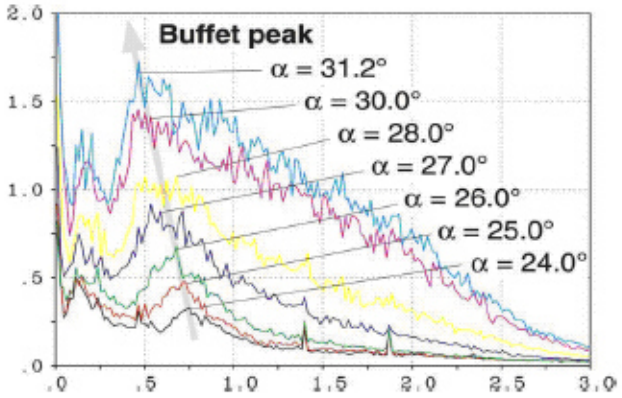

Figure 17: Fin buffet pressure Delta canard configuration

On this basis low speed fin buffet experimental results from measurements performed in the low speed wind tunnel of the TUM at 40 m/s on the

military trainer aircraft configuration can be applied for the validation of PVDF fin measurement results at Mach 0.5 from NLR HST wind tunnel as derived from the same mode, fig. 15 - 17.
As demonstrated below the locations MP9 and MP8 of the PVDF measurement are very close to the Kulite location P1 of the TUM experiment, see fig. 18. The location of MP11 is close to P2 and MP12 is near P3. Therefore for validation of the PVDF measured pressures comparison is performed using signals from similar locations.

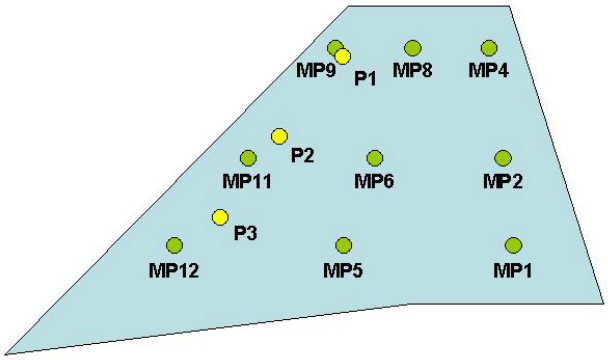

Figure 18: Comparison of pressure signal locations NLR (MP1-MP12) to TUM P1, P2 and P3

A comparison of c_{prms} values of NLR test signals MP9, MP8, MP11 and MP12 with TUM test signals P1 and P2 is depicted in the figure 5. The comparison in the range up to 30 degrees demonstrates that both the magnitude and the trend with incidence between the two different tests is in close agreement.

Good correlation is found for the c_{prms} buffet pressure values for all angle of attacks up to the limit of 30 ° which is present due to the limited TUM measurement program, see figures 19, 20 and 21. Small deviations might be due to calibration technique and different Mach number and cut off frequency.
As demonstrated by the variance and power spectra 8, 9 and 10, the PVDF PSD results show besides the peak at k~0.6 also a peak at k~1.2. Both peaks contribute to the overall rms value.

From this result of the comparison of the two different measurements it can be concluded that the PVDF measured buffet pressures, which are showing very similar magnitudes, are accurate enough to be used for prediction purposes.

Comparison of amplitude power spectra of the comparable signals from MP9, MP8 to P1, MP11 to P2 and MP12 to P3 lead to a similar conclusion.
In the table below peak pressure signals from power spectra are compared for the TUM signal P1 and NLR signal MP8. The amplitudes are similar. The difference results mainly from lower smoothing of the TUM signal which results in higher values. The rms pressure comparisons give a more precise picture.

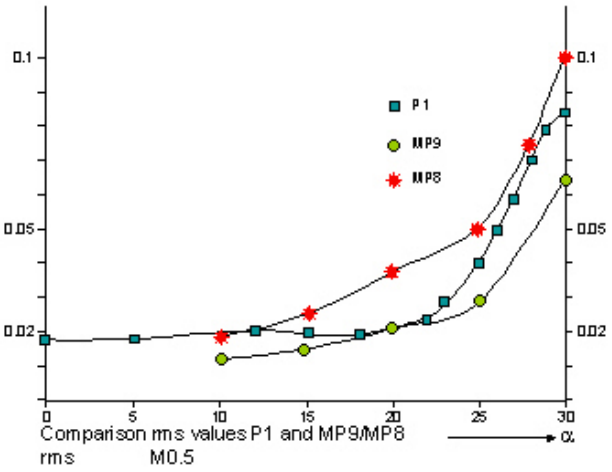

Figure 19: Comparison of $c_{p\ rms}$ from TUM test signal P1 with NLR test signals MP8 and MP9

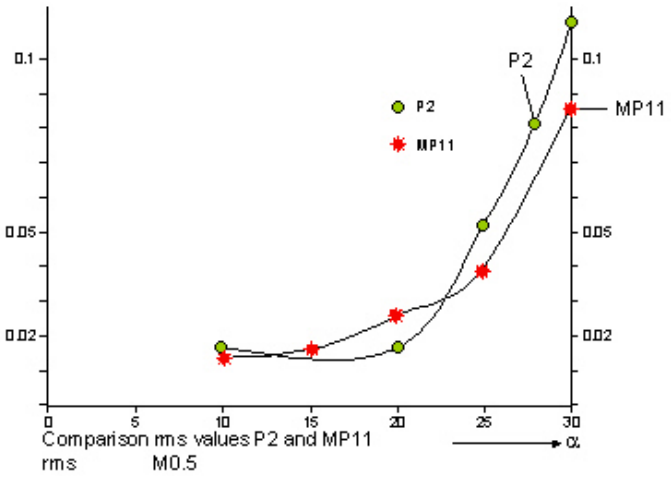

Figure 20: Comparison of $c_{p\ rms}$ from TUM test signal P2 with NLR test signal MP11

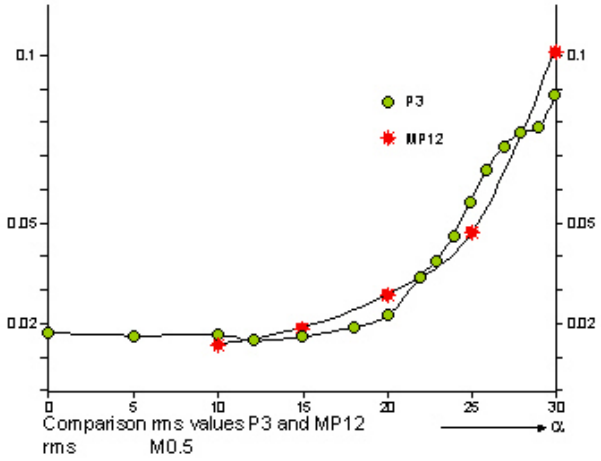

Figure 21: Comparison of $c_{p\ rms}$ from TUM test signal P3 with NLR test signal MP12

5. Recommendations

PVDF methods need special attention during calibration.
Application of the PVDF method for the derivation of unsteady buffet pressures during the development and design process of military structures is strongly recommended.

6. Conclusions

From the result of the comparison of the two different measurements it can be concluded that the PVDF foil technique is adequate for the application of the buffet prediction. This could be demonstrated through the validation of PVDF measured unsteady buffet pressures.

Furthermore it is concluded that the application of PVDF buffet pressure measurement technique leads to strong cost reductions compared to the classical approach during the design and certification of military aircraft structures including buffet dynamic loads. This is due to the fact that for the PVDF measurement the existing aerodynamic wind tunnel model for the derivation of stationary aerodynamic coefficients can be applied and it is not necessary to built an additional wind tunnel model for buffet as in case of the classical method.

	Peak Pressure signal	Reduced frequency	Incidence [deg]	$S_{cp\ max}$
NLR Trainer configuration	MP8	~0.6	10,0	0.000065
			30,0	0.0040
TUM Trainer configuration	P1	~0.6	10,0	0.00010
			30,0	0.0096

Table 4: Comparison of NLR and TUM measurements

7. References

[1] Luber W., Becker J., Sensburg O.
Impact of Dynamic Loads on the Design on European fighter
43rd Structures and Material Panel Conference, AGARD Florence 1996

[2] Becker J., Dau K.
Evaluation of vibration levels at the pilot seat caused by wing flow separation.
44th Structures and Materials Panel of AGARD, Lisbon, April 1977.

[3] Becker J., Gravelle A.
Some results of experimental and analytical buffeting investigations on a Delta wing.
Second International Symposium on Aeroelasticity and Structural Dynamics, AGARD SMP Aachen April 1985.

[4] Breitsamter C. and Laschka B.

Turbulent Flow Structure associated with Vortex Induced Fin Buffeting.
AIAA Journal of Aircraft, Vol. 31, No. 4, July-Aug. 1994.

[5] Breitsamter C., Laschka, B.
Aerodynamic Active Control For EF-2000 Fin Buffet Load Alleviation.
Proceedings of the 38th Aerospace Meeting &Exhibit, AIAA 2000-0656, 2000.

[6] Breitsamter C., Laschka, B.
Fin Buffet Load Alleviation Using An Actively Controlled Auxiliary Rudder At Sideslip.
Proceedings of the 22nd Congress of the International Aeronautical Council of the Aeronautical Sciences (ICAS), 2000.

[7] Schmid A., Breitsamter C., Laschka, B.
Charakteristic von Seitenleitwerk-Buffetlasten im Stall- und Poststall Bereich.
Deutscher Luft- und Raumfahrtkongress / DGLR-Jahrestagung,
Paper: DGLR-2001-068, Hamburg, Sept. 2001.

[8] J.K. Dürr, U. Herold-Schmidt, H. W Zaglauer, and J. Becker
Active Fin - Buffeting Alleviation for Fighter Aircraft
SPIE`s 6th Annual International Symposium on Smart Structures and Materials, Conference 3326,
March 1999, San Diego, USA

[9] Luber W., Becker J.
Comparison of Piezoelectric Systems and Aerodynamic Systems for aircraft Vibration Alleviation
SPIE`s 5th Annual International Symposium on Smart Structures and Materials, Conference 3326,
March 1998, San Diego, USA

[10] Becker J., Luber W.
The Role of Buffet in the Design of European Fighter
44th AIAA Structural and Materials Conference
April 2003, Hampton, USA

[11] W. Nitsche, M. Swoboda and P. Mirow
Shock dectection by means of piezofoils
Z. Flugwiss. Weltraumforsch. 15 (1991), 223-226, Springer Verlag

[12] Lee, I., Sung, H.J.
Development of an array of pressure sensors with PVDF film
Journal Experiments in Fluids, January 1999
Springer Berlin/Heidelberg, Volume 26, Number 1-2,

[13] R. Danz, B.Elling, A.Büchtemann and P. Mirow
Preparation, characterization and sensor properties of ferroelectric and porous Fluor polymers
11th International Symposium on Electrets, 2002

Copyright Statement